SOFT ROBOTS

3D-printed digital pneumatic logic for the control of soft robotic actuators

S. Conrad[1,2]*†, J. Teichmann[1,2]†, P. Auth[1], N. Knorr[1], K. Ulrich[1,2], D. Bellin[1], T. Speck[1,2,3], F. J. Tauber[1,2]*

Soft robots are paving their way to catch up with the application range of metal-based machines and to occupy fields that are challenging for traditional machines. Pneumatic actuators play an important role in this development, allowing the construction of bioinspired motion systems. Pneumatic logic gates provide a powerful alternative for controlling pressure-activated soft robots, which are often controlled by metallic valves and electric circuits. Many existing approaches for fully compliant pneumatic control logic suffer from high manual effort and low pressure tolerance. In our work, we invented three-dimensional (3D) printable, pneumatic logic gates that perform Boolean operations and imitate electric circuits. Within 7 hours, a filament printer is able to produce a module that serves as an OR, AND, or NOT gate; the logic function is defined by the assigned input signals. The gate contains two alternately acting pneumatic valves, whose work principle is based on the interaction of pressurized chambers and a 3D-printed 1-millimeter tube inside. The gate design does not require any kind of support material for its hollow parts, which makes the modules ready to use directly after printing. Depending on the chosen material, the modules can operate on a pressure supply between 80 and more than 750 kilopascals. The capabilities of the invented gates were verified by implementing an electronics-free drink dispenser based on a pneumatic ring oscillator and a 1-bit memory. Their high compliance is demonstrated by driving a car over a fully flexible, 3D-printed robotic walker controlled by an integrated circuit.

INTRODUCTION

The beginning of the 21st century is characterized by an ongoing fourth industrial revolution that is transforming interconnectivity within human society (*1*). Robots play a vital role in this transformation because they have increasing contact with their human counterparts (*2*). As this contact increases, so does interest and research in soft robotics (*3*–*6*). Being mainly made of polymer-based flexible components, these machines are safer for humans and more resistant to mechanical and chemical stress. In the future, soft robots could even work in extreme environments where radiation or acid would harm humans (or other organisms) as well as traditional metallic robotics (*4*).

A promising approach for driving soft machines are pressure-based actuators (*7*–*9*). Pneumatic grippers with passive shape adaptivity are one established example of such actuators because they handle fragile objects with different shapes in the packaging industry (*10*, *11*). Apart from these soft robotic hands, there is a growing number of experimental, pressure-based motion systems for walkers, crawlers, and other types of mobile devices. Today, there exists a wide selection of inflatable muscles and fingers (*6*, *12*–*14*), which make soft robots more adaptive and resilient in challenging environments.

To exploit the full potential of the inherent compliance of pneumatic actuators, it is of special interest to eliminate the need for rigid pressure control elements. Robot bodies can only be as compliant as their most inelastic structure, so they can benefit greatly from replacing parts such as metallic valves and printed circuit boards (PCBs). Proven alternatives for mechanical valves are regulators that use high voltage applied to flexible electrodes to manipulate an electrorheological fluid inside a channel (*15*, *16*). A variation in the voltage affects the viscosity of the medium. This way, electrodes along a tube can regulate the volumetric flow inside and block it completely. Another approach involving electricity is the design of valves based on dielectric elastomer actuators (*17*). Although flexible, these materials can perform linear expansion under high voltage and compress a fluid-carrying channel. Both strategies share the need for a high-voltage regulator nearby.

One approach that eliminates the need for any rigid electronics is using the pressurize medium itself to control its distribution to specific actuators (*18*). Pressure-triggered valves use the pressure level applied to one connector to regulate the volumetric flow between two others. Arranged in a network, this valve type acts analogously to electric metal-oxide-semiconductor field-effect transistors (MOSFETs) and can even perform digital operations (*19*, *20*). As a fully compliant alternative to classic solutions from microfluidics (*21*, *22*), Rothemund *et al.* (*23*) developed a soft cylinder that mimics the Boolean functionality of two coupled MOSFETs. These silicone-molded modules use a bistable membrane to control which of two tubes kinks (seals) or conducts air flow to an outlet (*24*). Depending on the exact configuration, the same valve can operate as different logic gates.

Rothemund and colleagues and following publications demonstrated the potential of their valve design by implementing fundamental circuits (for example, oscillators, storage modules, and digital-to-analog converters) (*25*, *26*) and including them in various applications (*27*). Drotman *et al.* (*28*) even used these modules to drive an electronics-free walker robot, and Kendre *et al.* (*29*) created a compatible software tool to design soft circuits. However, the high manual effort and the long manufacturing time limit larger

[1]Plant Biomechanics Group (PBG) Freiburg @ Botanic Garden of the University of Freiburg, Freiburg, Germany. [2]Cluster of Excellence *liv*MatS @ FIT–Freiburg Center for Interactive Materials and Bioinspired Technologies, University of Freiburg, Freiburg, Germany. [3]Freiburg Center for Interactive Materials and Bioinspired Technologies (FIT), University of Freiburg, Freiburg, Germany.
*Corresponding author. Email: stefan.conrad@biologie.uni-freiburg.de (S.C.); falk.tauber@biologie.uni-freiburg.de (F.J.T.)
†These authors contributed equally to this work.

implementations (*23*). Hubbard *et al.* (*30*) addressed this challenge and presented inkjet three-dimensional (3D) printable, fluidic transistors. Although getting rid of silicone molding is a big step toward a higher degree of automation, the described method still requires manual removal of support material and time-intensive flushing with a cleaning solution.

This study describes an entirely soft, fused deposition modeling (FDM) 3D-printed valve structure that operates as a pneumatic logic gate (PLG). Inspired by the work principle of Rothemund *et al.* (*23*), we combined the configurability and compliance of their module with an additively manufactured design and higher pressure tolerance. Our gate design aimed to simplify production by removing the need for manual fabrication and postprocessing. Circuits from such gates are shown to control electronics-free complex pneumatic systems. The compliance and robustness of our logic gates are highlighted in a fully flexible, electronics-free, integrated soft walker.

RESULTS

The logic gate design

The developed module (Fig. 1A) was 3D-printed from a thermoplastic polyurethane (TPU) filament with a shore hardness of A 63, A 70, or A 82. It consisted of two separate soft valves that controlled the airflow. These valves act analogously to an electric MOSFET, where a control signal (applied to the gate connector) manipulates the conductivity between two other connectors (source drain). These classic electronic MOSFETs can appear in a normally open (NO) or normally closed (NC) configuration, depending on whether they are conductive at a low- or a high-voltage level. The design of our soft valve was chosen to allow both configurations. The supplied air pressure acted analogously to the applied voltage level on a MOSFET. The single valve consisted of one big middle chamber, two parallel thin chambers, and a tube running through them (Fig. 1A). Expandable membranes of just 0.5 mm separated the chambers. In a pneumatic equilibrium, with equal pressure in all chambers, the membranes were relaxed and the tube allowed air to flow. If the side chambers received a higher pressure level than the middle chamber, the membranes between the chambers expanded inward, kinked the tube, and inhibited the airflow (Fig. 1, B and C). Depending on which chamber was defined as the "gate" of the valve, it enabled operation in different configurations. A NO configuration was achieved if the side chambers were connected to the control signal and the middle chamber was open to atmosphere as visible in V_1 (valve 1) (Fig. 1, B and C). In this mode, the valve allowed airflow when atmospheric pressure was applied to its gate and inhibited it when the signal switched to higher supply pressure (Fig. 1, B and C). The opposite behavior was observable when the middle chamber was connected as the gate of the valve and the side chambers were under permanently high pressure supply as shown in V_2 (valve 2) (Fig. 1, B and C). In this NC configuration, the valve was closed by an applied atmospheric pressure level and enabled air flow when it received overpressure (Fig. 1, B and C).

When combined into one integrated design (movie S1), the NO and NC valves formed a module that was able to mimic the functionality of electronic logic gates, which transformed Boolean input signals into a single Boolean output signal. In the PLG module presented here, atmospheric pressure (LOW) represented

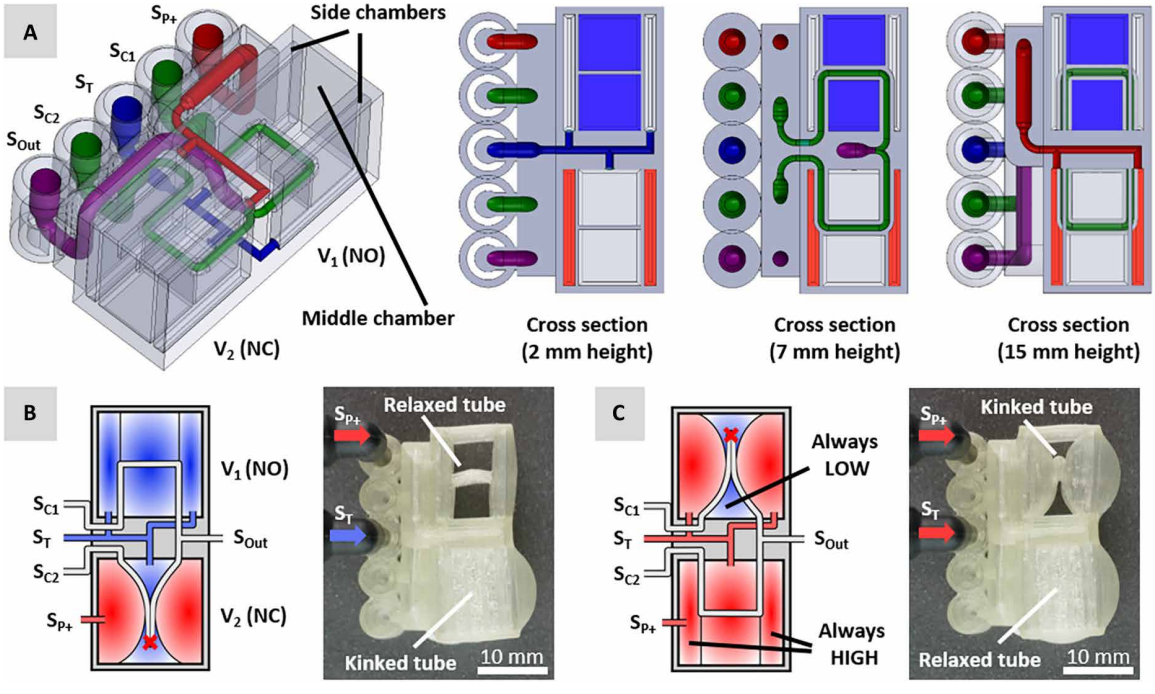

Fig. 1. Pneumatic logic gate. (**A**) Model and cross sections at varying heights of the PLG consisting of a NO valve (V_1) and a NC valve (V_2). Two sockets (S_{C1} and S_{C2}) supply input channels (green) leading through one valve each and merge in the output socket S_{Out} (purple). Because of a permanent pressure supply from S_{P+} (red), V_2 works in NC mode, whereas V_1 is NO. Accordingly, they operate alternately, controlled by the toggle socket S_T (blue). (**B**) Schematic illustration and physical PLG 3D-printed from TPU A 70 with a LOW signal applied to S_T. V_1 is open, whereas V_2 is closed, connecting S_{Out} to S_{C1}. (**C**) Schematic illustration and physical PLG with a HIGH signal applied to S_T. V_1 is closed, while V_2 is open, connecting S_{Out} to S_{C2}.

a digital 0, and a supply pressure level (HIGH) stood for a digital 1 (Fig. 1). The entire module was 3D-printed in one continuous process made of a TPU filament. It has a size of 37 mm by 26 mm by 18 mm, which originated directly from the geometry and material boundary conditions. The embedded tube necessitated an approximately circular cross section to seal shut when kinked. Therefore, the size had to be a compromise between maximizing volumetric flow and minimizing filament sagging. The minimum length of the straight tube part between the membranes was determined to be 8 mm based on the resulting inner diameter of 1 mm. To fully kink the tube, the membranes had to expand elastically by at least 2 mm. This necessitated membrane dimensions of 15 mm by 15 mm. The design presented in this work resulted from the combination of the dimensions of these elements and the physical sockets that are fitted to the size of the pneumatic connectors.

The PLG module contained five independent sockets (labeled S) for connecting pneumatic tubes (Fig. 1A). Because of the material's flexibility, the sockets provided a reliable, airtight hold for pneumatic connectors. S_{P+} (permanent pressure socket) was comparable to a Vcc (voltage at the common collector) pin on an electric device and was meant to be connected to a permanent pressure supply that pressurized the side chambers of the valve V_2 to maintain its NC configuration. Valve V_1 did not require an additional socket for staying in NO mode, because its middle chamber was open to atmospheric pressure by design. The control signal leading to the "gates" of both valves originated from a shared input socket S_T. Because the valves operated in opposite configurations, the control signal determined which of the two possible channel sockets (S_{C1} or S_{C2}) was connected to the output socket S_{Out} (Fig. 1, B and C, and movies S2 to S4). This way, the PLG operated as a pressure-activated three/two-way valve, allowing for diverse Boolean operations as elaborated in the subsequent sections. The tomography movies S2 to S4 show the effective kinking and sealing of the inner tube, as well as the changes during switching. For better illustration, the complex routing inside the module was reduced to a schematic 2D representation, which was used below to describe the PLG states and configurations (Fig. 1, B and C).

Operating pressure for single valve

The pressure limits of the described valves were determined by material and design parameters. To prevent damage, it was necessary to keep the pressure below the threshold of plastic deformation of the TPU membranes. However, the difference between the supply pressure and atmospheric pressure must still be high enough to cause membrane expansion, which inhibits airflow. To determine this self-sealing pressure P_{ss} for the valves, a supply pressure P_{sup} was applied to the channel and the side chambers of each separate valve. We studied the effect of P_{sup} on the resulting volumetric airflow $\dot{V}$ by varying the P_{sup} while the central chamber was left open to atmospheric conditions (Fig. 2A). When increasing the supply pressure P_{sup}, the TPU A 70 valves started sealing at 75 ± 5 kPa and could be considered as closed at pressure values of $P_{ss,V1} = 132 \pm 7$ kPa and $P_{ss,V2} = 115 \pm 11$ kPa (Fig. 2B). The highest observed self-sealing pressure was 148 ± 5 kPa, which makes 153 kPa the estimated minimum to ensure a reliable operation of the TPU A 70 valves. For TPU A 63, the averaged self-sealing pressure was found to be $P_{ss,V1} = 80 \pm 23$ kPa and $P_{ss,V2} = 73 \pm 14$ kPa. A shore hardness of A 82 raised these values to $P_{ss,V1} = 217 \pm 44$ kPa and $P_{ss,V2} = 235 \pm 44$ kPa.

The upper limit for a valve is its destruction pressure P_{dest}, which was determined by the toughness of the TPU material. By independently pressurizing each socket of the module while slowly raising the pressure, we were able to investigate under what load the membranes would fracture (table S1). The tested TPU A 70 modules ($N = 30$) showed a median destruction pressure P_{dest} of 500 ± 20 kPa. The observed minimum lay at 420 ± 20 kPa, leading to the definition of a recommended pressure limit of 400 kPa for TPU A 70 valves. In comparison, valves made of TPU A 63 experienced a membrane failure averaged at $P_{dest} = 310 \pm 30$ kPa with an observed minimum of 260 ± 20 kPa. Valves printed with TPU A82 filament withstood a pressure of more than 750 kPa, which was the maximum our test setup could provide.

Operating pressure for logic gate

When two valves worked antagonistically in a logic gate module, the system's Boolean behavior highly depended on the supply pressure. To achieve distinct HIGH and LOW states, the NO V_1 and the NC

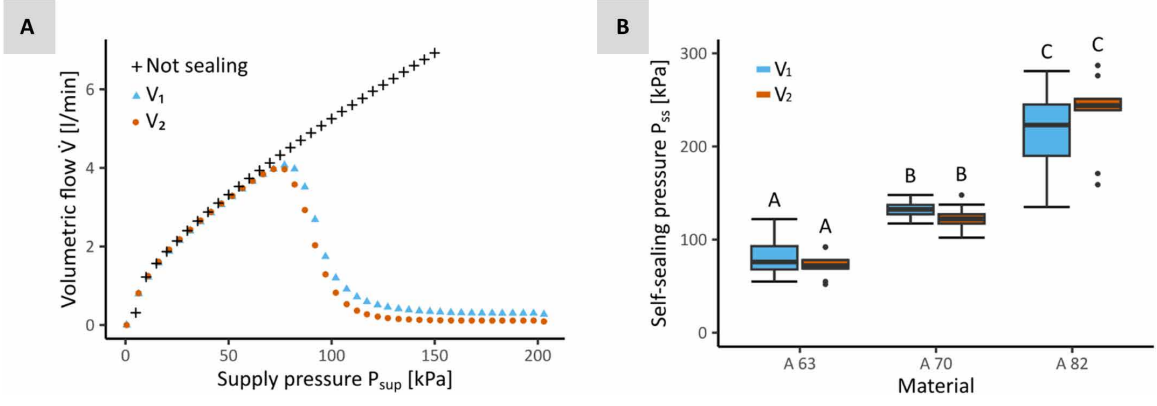

Fig. 2. Self-sealing pressure of the PLGs. (**A**) Measurement of the volumetric flow through the TPU A 70 valves V_1 (triangles) and V_2 (dots) in dependency of the applied supply pressure P_{sup}. With pressure applied to the gate connector, both valves show reduced flow above 75 kPa compared with the unobstructed flow curve (crosses) ($N = 20$). (**B**) Self-sealing pressure measured for TPU with varying shore hardness. Different letters indicate significant differences where $P \leq 0.05$ in the two-way analysis of variance (ANOVA) test with Tukey's range test as post hoc test ($N = 20$ for A 70 and $N = 9$ for A 63 and A 82).

V_2 were designed to never allow air flow at the same time. Simultaneous connection could occur when a switching input signal on S_T caused one valve to close before the other opened. For the closing pressure P_C of the valves, this resulted in the criteria of Eq. 1

$$P_{C,V1} < P_{C,V2} \quad (1)$$

Assuming the pressure applied to the tube inside a valve had negligible influence on its closing behavior, the closing pressure of V_1 equaled its self-sealing pressure P_{ss}. For the NC valve V_2, the closing pressure P_C rose linearly with the supply pressure P_{sup}. This was due to its membranes expanding as a result of the pressure difference between the side chambers and middle chamber, as shown in Eqs. 2 and 3

$$P_{C,V1} \approx P_{ss,V1} \quad (2)$$

$$P_{C,V2} \approx P_{sup} - P_{ss,V2} \quad (3)$$

According to Eq. 4, this led to a predicted minimal supply pressure that was the sum of the self-sealing pressures of V_1 and V_2

$$P_{sup} > P_{ss,V1} + P_{ss,V2} \quad (4)$$

For the determined TPU A 70 values of $P_{ss,V1}$ and $P_{ss,V2}$, this resulted in $P_{sup} > 247 \pm 10$ kPa. We verified this by measuring the volumetric flow separately through V_1 and V_2 as a function of the input signal P_A. An intersection between the falling flow curve of V_1 and the rising curve of V_2 indicated an undefined state of the logic gate in which S_{C1} was directly connected to S_{C2}. The overlap decreased with a rising supply pressure P_{sup} (Fig. 3, A and B). If both channel sockets received different pressure levels in that moment, the result would be an unintended airflow. The width of the transition interval for rising and falling pressure lay between 40 and 60 kPa (fig. S1). The observable hysteresis between opening and closing was caused by the walls sticking to each other when the tube was kinked because of adhesive forces at the polymer surface.

We confirmed these anticipated losses during a switching state on S_T in an additional experiment. By sealing S_{Out} and connecting S_{C1} to a pressure source, we were able to investigate the dependency between P_{sup} and the volumetric flow $\dot{V}$ when switching S_T from LOW to HIGH (Fig. 3C). On the basis of the results, we chose 225 kPa as the optimal supply pressure for the PLG and used this value for further characterizations. For pressure levels between 132 and 225 kPa, the PLGs still operated well as long as the pressure source was able to provide the additional volume required by the described unintended airflow.

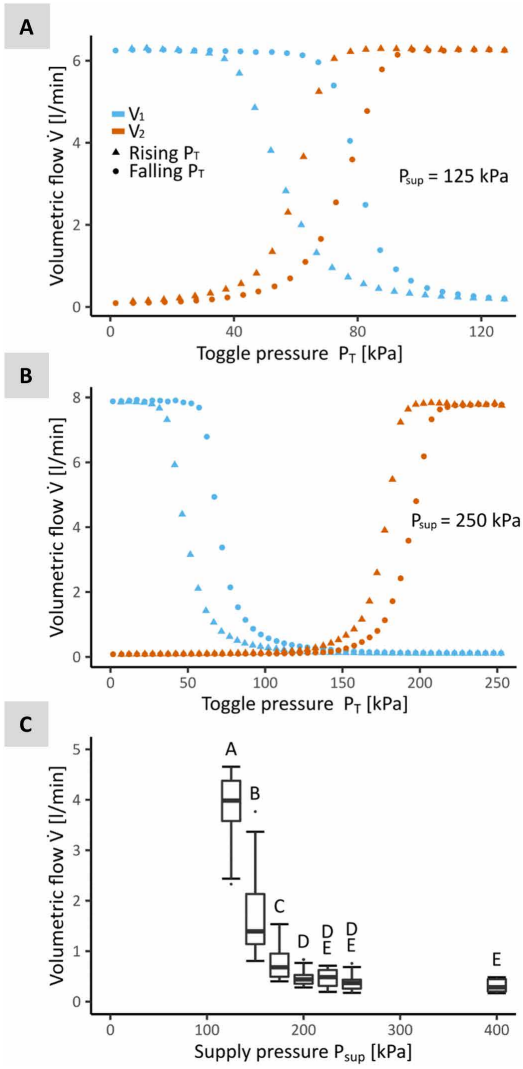

Fig. 3. Switching behavior of A 70 PLGs in dependency of the applied supply pressure P_{sup}. A rising toggle pressure P_T (triangles) causes valve V_1 to close, whereas it opens valve V_2. A falling signal (dots) has the opposite effect. (**A**) Opening and closing of V_1 (blue) and V_2 (orange) at 125 kPa shows a pronounced overlapping. (**B**) Opening and closing of V_1 and V_2 at 250 kPa are separated ($N = 1$). (**C**) Peak volumetric flow during a switching input signal at the S_T socket. The measured flow falls with a rising supply pressure and does not change significantly anymore for $P_{sup} > 225$ kPa. Different letters indicate significant differences where $P \leq 0.05$ in the Mann-Whitney U test with Wilcoxon signed-rank test as post hoc test.

Logic gate configurations

The PLGs were able to operate as different logic gates whereby the toggling connector S_T was always defined as input A. Depending on the assignment of high pressure (HIGH = logic 1), atmospheric pressure (LOW = logic 0), or a second input signal B to the channel connectors S_{C1} and S_{C2}, the module could be configured into a logic OR, AND, or NOT gate.

Inspired by the results of Rothemund *et al.* (*23*), we applied supply pressure to S_{C1} and atmospheric pressure to S_{C2} to realize a NOT gate (Fig. 4, A and B). The logic NOT had only one input and inverted the incoming signal. The output Q was pulled to HIGH as long as the input A was LOW because permanent pressure was led through V_1 and V_2, inhibiting the flow out. When A switched, the HIGH signal was blocked by the now-closed V_1, and the pressure escaped through the open V_2 (Fig. 4, C and D).

To configure the module as an AND gate, we applied atmospheric pressure to S_{C1} and introduced a second input B connected to S_{C2} (Fig. 5, A and B). The logic AND outputted a LOW signal unless both input signals were switched to HIGH. The PLG achieved this by leading the input signal B through the NC valve V_2. As long as A stayed LOW, the output was permanently connected to atmospheric pressure. When A turned HIGH, the resulting output started to depend on B. If B was HIGH as well, a HIGH signal was obtained on Q (Fig. 5, C and D).

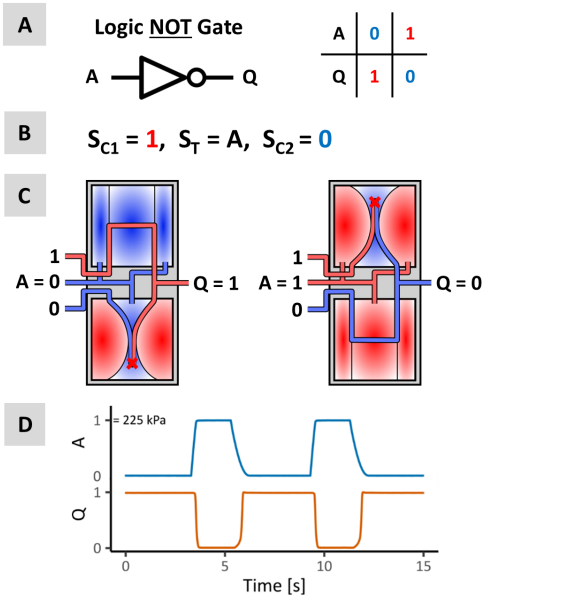

Fig. 4. Description of the pneumatic logic NOT gate. (**A**) Circuit symbol and logic table of a NOT that inverts the input signal. (**B**) Signal assignment defining the gate's type. The NOT only requires one input and two permanent pressure levels. (**C**) Schematic illustration (S_{P+} removed for simplification) of the two possible states for this gate. Determined by input A, the output Q is connected to either the HIGH or the LOW signal. (**D**) Measured pressures of A switching state and the response of Q.

To turn the module into a logic OR, we moved the input B to V_1 and supplied S_{C2} with constant pressure (Fig. 5, E and F). Unlike the AND gate, for an OR, a HIGH signal on one input was already enough to output HIGH. As long as A was LOW, the returned signal on Q depended on B. A HIGH signal on A made B negligible and connected the permanent pressure supply to the output, pulling its signal to HIGH (Fig. 5, G and H). Observable nonlinear behavior in the measured data originated from noise of the pressure supply in moments of fast changes in the volumetric flow.

Response time

An important feature of a logic gate is its response time, wherein a changing input signal causes a reaction at the output. To determine this response time t_{res}, we configured the module to form a buffer. A buffer is a switch that outputs the incoming signal of a single input A and could be built by swapping the signals of S_{C1} and S_{C2} on a NOT gate (Fig. 6A). By connecting up to five of these switches in series, we were able to measure the time it takes an initial input to propagate to the last output (Fig. 6, B and C). The delay rose proportionally to the number of modules and increased for higher supply pressures. The response time t_{res} for a single gate at P_{sup} = 225 kPa was 106 ± 6 ms for a switch from LOW to HIGH and 96 ± 33 ms for a switch from HIGH to LOW.

Further configurations

For the presented PLG design consisting of two antagonistically operating valves (Fig. 1), seven signal assignments created a meaningful binary operation (fig. S2). Besides the three characterized configurations, there was one more variant for AND and OR, where the constant signals were replaced by the input A. This was possible because in this configuration, input A only affected the output if it was in the formerly constant state. Furthermore, there were two configurations whose logic tables represented the known AND and OR gates with an inverted input A. Gates like NAND, NOR, and XOR were not possible with two pneumatic valves but could be realized with combinations of the presented gates.

Resilience

To determine the physical limitations of the developed modules, we characterized their cyclic behavior and response after compression experiments. By periodically changing the input signal on the toggle socket S_T from 0 to 225 kPa and back, we simulated the switching in a long-term operation. The PLGs showed an averaged endurance of 6528 ± 4420 cycles (N = 10) before failure. All tested modules ruptured at the outer wall or the ceiling of valve V_2 (table S2).

In a separate experiment, we investigated the mechanical durability of the PLGs. The modules were compressed in a universal testing machine with 3, 6, or 9 kN along their three axes (movie S5). After each compression step, we characterized their volumetric flow and their response times. Although the plastic was visibly deformed in x-ray microtomography images of three exemplary PLGs (fig. S3), all PLGs withstood the full load of 9 kN. Furthermore, they revealed no qualitative decrease in the volumetric flow passing (fig. S4) through their channels nor a decrease in response times to changing input signals (fig. S5).

Electronics-free drink dispenser

To demonstrate how our logic gates are able to replace electrical control circuits, we built a fully pneumatic drink dispensing system (Fig. 7). A 3D-printed peristaltic pump transported fluid from a reservoir up into a beaker placed on a platform. The pump was based on the peristalsis of the esophagus (*31*). It was driven with 225 kPa by a periodic pattern that sequentially closed and opened eight independent segments in the transport direction. The pattern was generated by a pneumatic circuit that used seven buffers to forward a signal, after which it was passed back to a NOT gate that inverted it (Fig. 7A). Together, these eight PLGs formed a ring oscillator that periodically switched eight independent output signals. By connecting one signal to each segment of the pump, the circuit caused a full closing cycle from the bottom to the top before it started opening again. To stop the oscillation, the output signal of the last buffer is fed through an OR gate before returning to the NOT module. For example, the pump circuit could be controlled by a set-reset (SR) latch, which processed the incoming signals from an industrial pneumatic push button and a 3D-printed weight sensor. Pressing the button sent a LOW signal to the SET input of the latch, which changed its output signal to LOW. This then activated the peristaltic pump by allowing the oscillating signal to pass the OR gate. The water level in the beaker rose, causing an increase in the load on the platform. The weight sensor below the platform consisted of a compliant lever and a pressurized tube that kinked when the lever bent under the increasing force. As soon as the load obstructed the airflow in the tube, the pressure at the sensor output dropped because of a small hole acting as a pulldown resistor, and the latch received a LOW signal on its RESET input (Fig. 7B and movie S6). This switched its output back to HIGH, and the ring oscillator was deactivated, because the LOW signal could not pass the OR gate anymore. The device stayed idle until the full beaker was removed, and

the start button was pushed again. While the push button was actively pressed, the latch would always output a LOW signal because of its specific implementation using two AND gates. In this state, the dispenser ignored a triggered sensor, which allowed the users to top up the fill level of the beaker if they desired.

Fully integrated compliant walker

The drink dispenser demonstrates possible logic operations and shows how they drive a periodic process with user interface and sensing. However, it is still a stationary machine mounted on a rigid frame. To highlight the advantages of material softness and stress resilience, we embedded our PLGs in a fully integrated, entirely flexible robot that walked under applied air pressure (Fig. 8). The 76.5-g device was 3D-printed with flexible TPU A 70 (Fig. 8A) in one continuous process and did not require any manual intervention or further assembly. After a fabrication time of 50 hours 22 min, it was easily removed from the build plate. It started walking when a pressure source was connected to its single socket. Because of its high compliance, the walker was capable of withstanding multiple impacts during operation (Fig. 8B and movies S7 to S9). The device walked in a trot-like gait (Fig. 8, D and E, and movie S10) using two pairs of diagonally connected legs (Fig. 8C). Each leg repeated a sequence of up-forward-down-backward movements, performed by three independent pneumatic actuators. Hereby, horizontal deformation resulted from two antagonistically operating actuators (Fig. 8C). The vertical bending of the leg was realized by one actuator working against flexible ligaments, which acted as a spring pulling the leg up again when the actuator relaxed.

The motion pattern was generated by an oscillator circuit consisting of three NOT gates in the central body of the robot. The output of each NOT gate was connected to one of the three inflatable actuators inside each leg (Fig. 8C) with a phase offset of 120° between the two pairs of legs. The pneumatic signals were forwarded and split by 1-mm channels inside the walkers' body. Supplied by 175-kPa pressurized air, the robot walked with an average speed of 33 mm s^{-1}, which corresponds to 0.25 BL s^{-1} (body length per second) (Fig. 8, D and E). Although the device lifted its body only slightly, it was still able to carry up to 3.7 times its own weight (285.5 g). Under this load, it moved 12 mm s^{-1} and was still stable enough to balance objects placed on top (movie S11). Equipped with a CO_2 cartridge and a pressure regulator (479.2 g) on its back, the untethered walker crawled forward at speeds of 9.5 mm s^{-1}, corresponding to 0.07 BL s^{-1} (movie S12). To demonstrate the resilience of a fully compliant robot, we performed a series of load and impact tests (Fig. 8B). The walker was stepped on by a 70-kg person, run over by a 1800-kg car, and impacted with 12 J (movies S7 to S9). It withstood all loads and showed no change in speed or gait afterward.

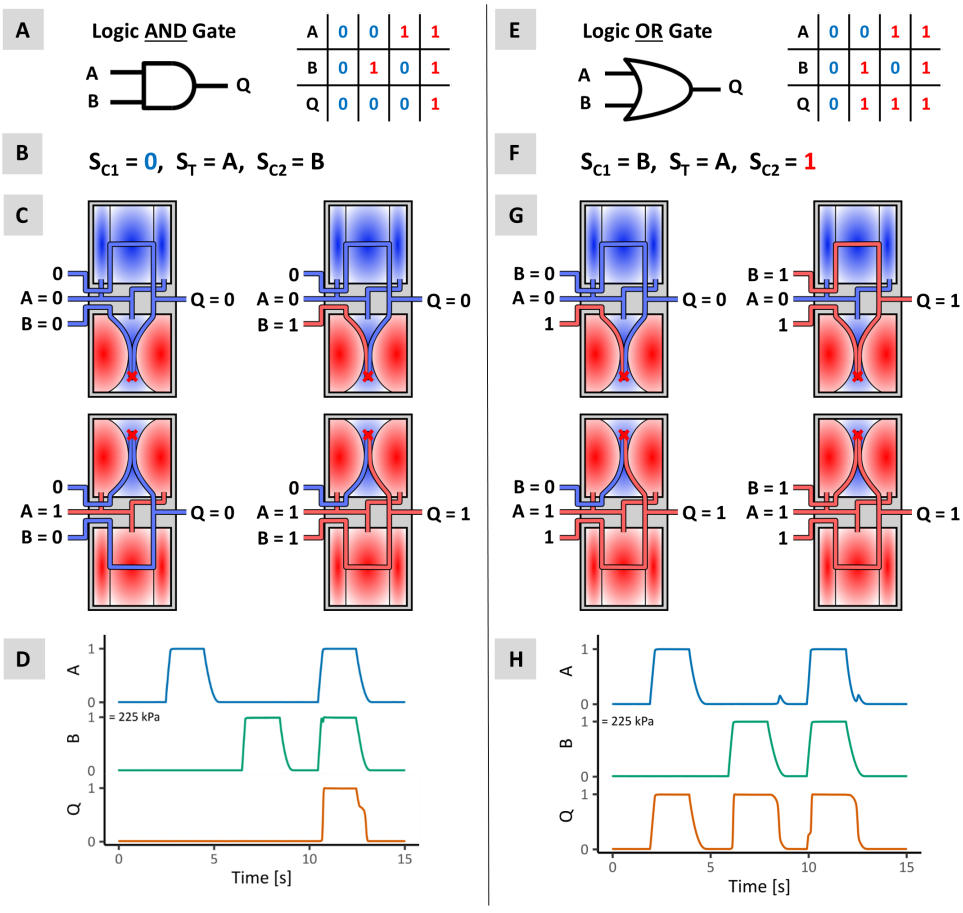

Fig. 5. Description of the pneumatic logic AND and OR gates. (**A**) Circuit symbol and logic table of an AND that only returns HIGH if both input signals are HIGH. (**B**) Signal assignment defining the gate's type. The AND requires two inputs and a permanent supply of atmospheric pressure. (**C**) Schematic illustration (S_{P+} removed for simplification) of the four possible states for this gate. Depending on A, the output Q is conducted to a LOW signal or receives the signal from input B. (**D**) Measured pressures at A, B, and Q during all combinations of input states. (**E**) Circuit symbol and logic table of an OR that returns HIGH if one of the input signals is HIGH. (**F**) Signal assignment defining the gate's type. The OR requires two inputs and a permanent supply of high pressure. (**G**) Schematic illustration (S_{P+} removed for simplification) of the four possible states for this gate. Depending on A, the output Q is conducted to a HIGH signal or receives the signal from input B. (**H**) Measured pressures at A, B, and Q during all combinations of input states.

DISCUSSION

The 3D-printable compliant modules described in this work consist of two pressure-triggered valves that mimic the work principle of an electric MOSFET. They rely on a three-chamber system that uses pressure-actuated membranes to kink a tube between them and therefore control the airflow. By configuring one valve as NO and the other as NC, it is possible to build a device in which the state of an output signal is determined by the input signals according to the logic tables of AND, OR, and NOT gates. Hereby, the general work principle and the signal assignments follow the suggestions of Rothemund *et al.* (*23*, *25*). However, they discussed the urgent need for a faster and less complicated fabrication method to achieve larger implementations and a wider use of soft logic. Our

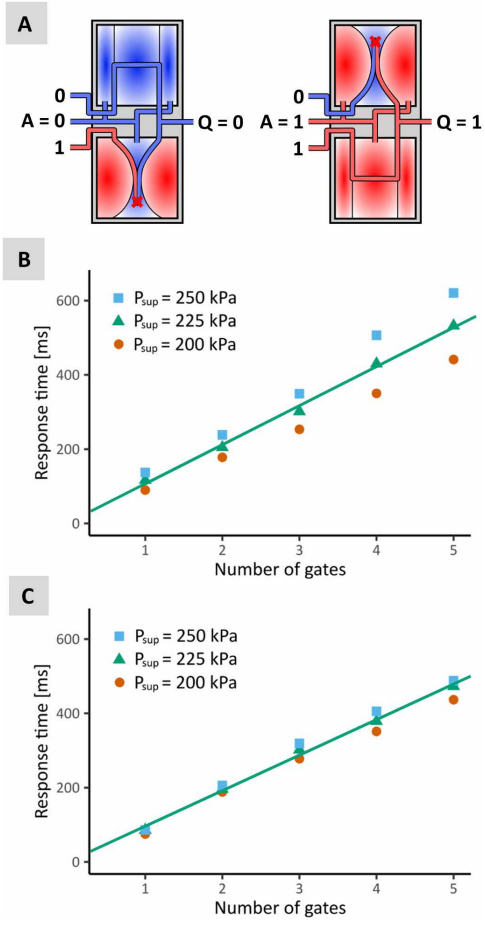

Fig. 6. Measured propagation time of an incoming signal through a series of A 70 buffers under different supply pressures. ($N = 10$) (**A**) Signal assignment for a buffer (S_{P+} removed for simplification). (**B**) Response times for a switch from LOW to HIGH. (**C**) Response times for a switch from logic HIGH to LOW. All response times show a strong linear trend, increasing with the number of gates ($R^2 > 0.99$).

device solves this challenge because it uses an innovative design, making it entirely 3D printable. The fabrication process takes 7 hours without requiring any user intervention or postprocessing because no support material is needed. We demonstrated that flexible channels with an inner diameter of 1 mm and membranes of 0.5-mm thickness are printable with regular FDM technology. This benefit minimizes manual effort and accelerates the design and test cycle for next module generations.

The characterization of the PLGs showed that pressure limits and tested materials are related. Reliable valve operation for TPU A 63 was found between 80 and 260 kPa, because valves with shore hardness of A 70 work between 153 and 400 kPa. Valves using TPU A82 operate at a minimum of 235 kPa with an upper limit of more than 750 kPa. This trend can be explained by the effect of reduced elasticity on expansion behavior under pressure. When the elasticity decreases, the material can resist more force before it fails, but it also needs a higher pressure to stretch. Because the module design and membrane thickness remained constant in all experiments, a greater shore hardness resulted in a higher minimum required pressure difference between the side chamber and middle chamber to seal the tube. This explains why not only the maximum but also the minimum pressure depends on the chosen filament. The TPU A 70 modules were selected for further characterization because this material was able to achieve high reliability in 3D printing while maintaining acceptable flexibility and therefore low air pressure requirements.

Our logic gates have a higher operating pressure than comparable approaches, which is a result of the comparatively high shore hardness of our TPU versus the silicones typically used for molding. Although this disqualifies our device for low-pressure applications, it enables the control of high-pressure actuators requiring supply pressures of 200 kPa and higher (*32*–*35*). Compared with the valve presented by Rothemund *et al.* (*23*), our modules require a supply pressure that is about one magnitude higher. Rothemund *et al.* characterized their gates at 15 kPa, and Preston *et al.* (*25*) specified their limit at 50 kPa. In contrast to our module, the silicone gate does not need to avoid an overlapping state between both valves. Because of the bistable behavior, no simultaneous airflow through both valves is possible, and unintended leakage is excluded.

One result of the higher supply pressures of our TPU valves is response times around 100 ms. This is markedly faster than the values measured for the silicone valve presented in the supplementary materials of Preston *et al.* (*25*), which showed durations between 250 and 1000 ms. Although the results are not directly comparable because of the different pressure levels, our PLGs would be advantageous in time-critical applications. The response times of the silicone valve decrease as the supply pressure increases, whereas our device exhibits the opposite behavior. The reason for this is the different closing principles. In our case, the incoming pressure opens the NC valve by working against the side chambers according to Eq. 3. Building up this pressure takes longer the higher the supply pressure is. However, higher pressure tolerance and faster response times are only advantageous depending on the desired application.

Our module is of comparable size to the bistable valve from Rothemund *et al.* (*23*), and it covers the same range of logic operations. Our design uses two alternately acting independent valves, which enable signal assignments for essential logic operations that are necessary to build any complex circuitries. Other configurations result in variants of these logic modules but do not cover the full range of possible logic tables. Gates like NAND, NOR, and XOR cannot be implemented with the presented design. They will require a more complex module or combinations of multiple gates.

Although the silicon valve has a similar work principle, it can perform two tasks that our module cannot yet perform. Because of the bistable membrane (and the resulting inherent Boolean behavior), the valve can be combined with a cavity to form a single-valve oscillator (*23*). The current design of our PLG cannot achieve such a simplification. Because of its bistability and design, a valve by Rothemund *et al.* can also be used as a button or as a 1-bit memory storage device, which is not possible with our current PLG design.

However, our approach offers an automated rapid fabrication method, modifiability, and ease in testing new PLG designs, all of which will be highly valuable for many applications. This is especially true when developing complex systems, which require multiple, fast iteration cycles. The resilience test results support a wide range of possible tasks, because the compression tests revealed no substantial decrease in performance even after a load equivalent of 900 kg was applied.

We combined our modules in various configurations and constructed a circuit that not only implements a time-delay ring

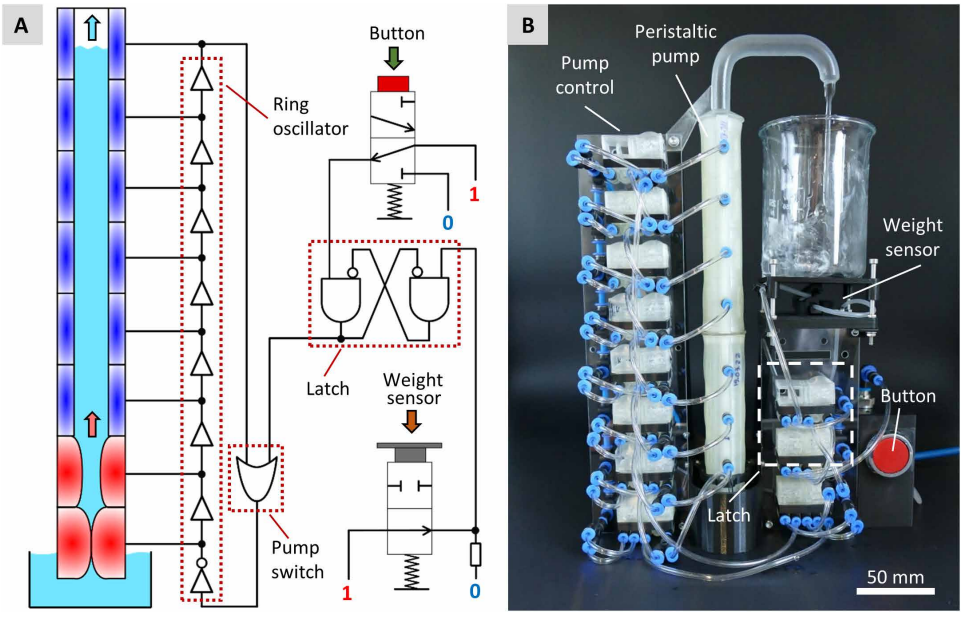

Fig. 7. Drink dispenser driven by PLGs. (**A**) Schematic diagram of the pneumatic circuit. A peristaltic pump is sequentially closed and opened by an oscillator made of seven buffers and one NOT gate. It is controlled by a latch that processes the input from a start button and a weight sensor. (**B**) Implemented test stand for the drink dispenser. Eight PLGs on the left side form the oscillator. If the weight sensor below the cup triggers, it switches the latch and the pump stops.

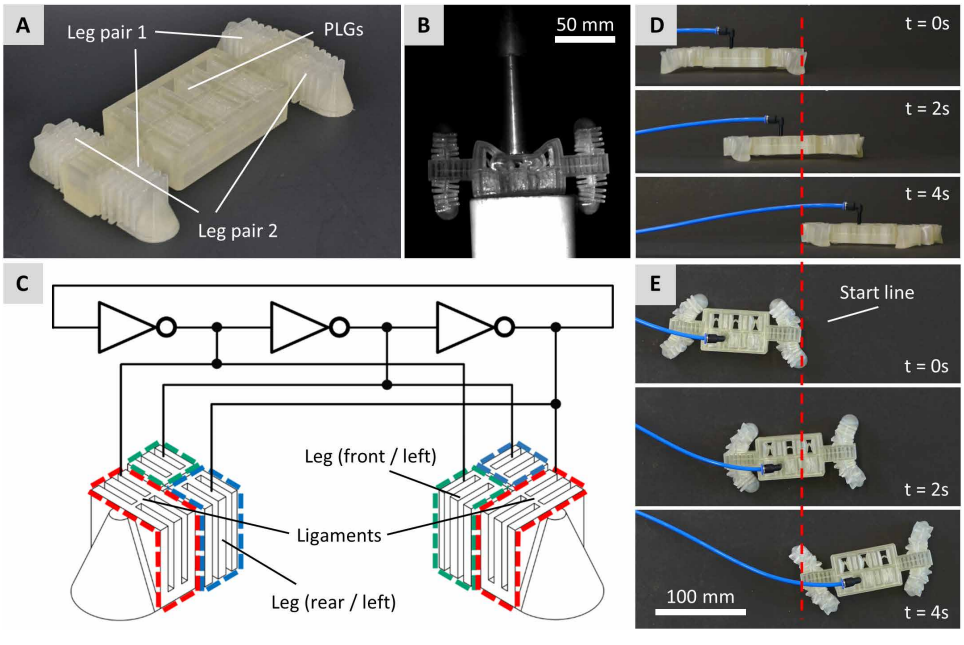

Fig. 8. Compliant walker driven by PLGs. (**A**) Integrated, compliant walker 3D-printed with TPU A 70. (**B**) Impact test on the walker with a 500-g weight dropped from 2.5 m. (**C**) Oscillator circuit connected to two independent pairs of legs. The displayed legs represent the two diagonally coupled pairs. Each leg consists of three actuators to bend forward (green), backward (blue), and down (red). (**D**) Side view and (**E**) top view on the walker's motion pattern. The walking speed of the unloaded robot is 0.25 BL s^{-1} (33 mm s^{-1}).

oscillator but also uses this sequential switching to drive a peristaltic pump. Combined with an OR gate (acting as a digital switch) and an SR-latch circuit, the demonstrator forms an electronics-free drink dispenser. Using the buffer as a 1-bit memory, it can distinguish between on and off states and respond to signals from a start button and a pneumatic weight sensor. The demonstrator contains all the basic gate configurations, as well as feedback circuits, sensor technology, and a user interface. In this way, it demonstrates how devices controlled by pneumatic logic can replace complex electrical machines.

Whereas the drink dispenser shows how the PLGs can compete with their electric counterparts in terms of functionality, our second prototype highlights the advantages of 3D-printed soft modules over ridged PCBs. The fully integrated four-legged walker requires no manual assembly after printing and can be activated in a plug-and-play style. The walker's ability to withstand various compression and impact tests and its relatively high speed even under substantial loads qualify it for various tasks that require the fast, automated production of small transport vehicles. Compared with the soft-legged quadruped robot presented by Drotman *et al.* (*28*), our walker demonstrated competitive characteristic values. With 0.07 BL s^{-1}, the untethered version of the device has a similar relative motion as the quadruped robot reaching 0.09 BL s^{-1}. Compared with its tethered version (0.13 BL s^{-1}), our tethered walker reaches almost twice the speed (0.25 BL s^{-1}), although the two versions cannot be directly compared because this robot uses electromechanical components (*36*, *37*).

On the basis of the results of the cyclic behavior and response time experiments, the pump could transport water for an average time of 4 hours, and the walker could walk approximately 2 hours before the PLGs would need to be replaced. These numbers illustrate the need to further improve the PLG design and the fabrication technique. Because all material failures happened on the outer shell of the module, it is likely that their resilience against cyclic loads could be increased by thickening the affected walls. The internal membranes, although thinner, are restricted in their expansion by the available space and therefore never failed before the external features. The wide spread in the distribution of failure cycles indicates quality deviations in the fabrication process. An enhanced FDM 3D printing of filaments with low shore hardness would not only help to make pneumatic logic more durable but also reduce the variation between the single modules.

The goal of this study was to develop innovative PLGs that overcome the challenges of existing approaches (for example, complexity, manual effort, and pressure tolerance). The presented module is designed to be manufactured using commercially available filaments on regular FDM 3D printers, which enable a time-efficient and automated production. The completely flexible structure, made of a single material, contributes to its robustness and sustainability. Both improvements will speed up the prototyping of new module generations and will simplify their direct integration into larger circuits. We showed how the chosen material influences the working range, which provides another degree of freedom to fit the developed modules to specific future applications.

Depending on the signal assignment, the gates operate as logic AND, OR, and NOT and have proven to be reliable in essential feedback circuits like oscillators and latches. The gate's tolerance of high supply pressure opens the application space for actuators whose requirements overextend silicone-based valves so far. We demonstrated a practical application with an electronics-free drink dispenser based on a peristaltic pump, which requires adequate pressure to fully close its segments. A mobile walker robot further highlighted the potential of fully integrated circuits, because they are ready to use directly after being taken out of the printer without any further effort. The load tests show high durability not only of individual PLGs but also of complex systems that are driven by them. The walker could not only withstand several impacts while walking but could even survive being run over by a car without damage. In the future, such systems could be deployed in search-and-rescue scenarios in which electronic systems could fail, be crushed, or harm persons.

The size of the logic modules is mainly determined by the flexibility of the membranes, so future improvements in FDM printing may allow for further miniaturization. The next steps for this research will be the redesign of the presented PLGs to compensate for existing weak spots and the construction of new gate geometries that include four valves to enable the full range of fundamental logic operations. A future simulation of the fluid dynamics inside the module in interaction with its pressure-induced deformation will contribute to the optimization of the channels and chambers. In addition, we will focus on further improving the fabrication process so the FDM 3D printing can unfold its full potential for creating complex compliant geometries. This is a next step for pneumatic logic to replace more and more complex electric components in soft robots.

MATERIALS AND METHODS

Fabrication

The described pneumatic elements were fabricated on a 3D printing platform as detailed by Conrad *et al.* (*38*). The system has already proven its potential for handling filaments with low shore hardness and has created several innovative pneumatic actuators (*39*, *40*). The flexible parts, like valves and logic gates, described in this work have been printed in one continuous process with "Recreus FilaFlex TPU A60" (shore hardness A 63) (*41*), "Recreus FilaFlex TPU A 70" (*42*), and "Recreus FilaFlex TPU A 82" (*43*) with fitting print parameters (table S3). This includes pneumatic connectors, channels, and expandable membranes. The values were chosen to put as little force as possible on the flexible filament to prevent it from kinking and bending inside the extruder. Most parameters were set in the software PrusaSlic3r 2.4, which was used to prepare our models for printing. In a postprocessing step, the files generated by the software were additionally modified to adapt the flow rate to the special needs of the flexible filament. Because no support is needed, the logic gate is ready for use directly after printing (Fig. 1A). After connecting tube adapters to the flexible sockets, the module can be inserted into a pneumatic circuit.

Specified logic gate design for FDM 3D printing

Because the valve and final logic gate are supposed to be manufactured on an FDM 3D printer, their design was fitted to the requirements of this fabrication method. TPU A 70 is a very flexible filament that easily bends and gets tangled inside the extruder. To avoid this and ensure an optimal flow, the device was printed on low speed with 10 mm/s and with a temperature (230°C) that is at the upper limit for this material. Despite choosing these basic parameters, it was still challenging to create airtight bonding between all layers. One way to enhance the connections is to set an increased flow rate (over extrusion). However, this usually also results in swelling and sealed channels in such a detailed object. Introducing an adapted extrusion factor solved this problem (table S3). By doing so, just the flow rate on perimeters and membranes was increased while every other part of the pneumatic element was printed normally. Because FDM-printed TPU A 70 cannot reliably build overhanging walls, all chambers were designed to be rectangular. Membranes were designed vertically and straight between two thicker regions as anchor points, and the ceiling of a chamber was at least 2 mm thick to ensure smooth, tight layers after the porous bridging. Because thin holes are a challenge for FDM printers, the vertical channels inside the logic gate had a diameter of 2 mm, whereas horizontal channels needed only 1 mm.

Testing methods

To characterize the logic modules and to determine their working conditions, different operating pressures and gate configurations were tested. In all pneumatic experiments, the pressurization of chambers and channels was controlled by a custom test stand. This setup contained six pneumatic proportional valves driven by a LabView program. The software supports the creation of linear patterns and repeating sequences, which simplified the systematic characterization by applying rising and falling pressure ramps to the logic elements. For the characterization of a single valve, unused inlets were sealed, and the gate output socket was connected to atmospheric pressure via a flow sensor to measure the volumetric stream. After changing the state on the input connectors, the software waited 4 s for the module to reach a new static internal flow and then recorded this value. To test the behavior of the complete logic gate, a pressure sensor was connected to the output. Here, the applied pressure was measured continuously to characterize the dynamic behavior.

For deformation experiments, we used a mechanical testing machine equipped for compression tests up to 10 kN and a drop tower that allows acceleration of a defined mass before it hits the target. The compression tests were executed with a velocity of 24 mm min^{-1} (movie S5). The velocity and motion pattern of the walker robot were characterized with the help of video equipment.

Supplementary Materials

This PDF file includes:

Materials and Methods
Figs. S1 to S5
Tables S1 to S3
Legends for movies S1 to S12

Other Supplementary Material for this manuscript includes the following:
Movies S1 to S12
Data file S1

REFERENCES AND NOTES

1. S. Robla-Gomez, V. M. Becerra, J. R. Llata, E. Gonzalez-Sarabia, C. Torre-Ferrero, J. Perez-Oria, Working together: A review on safe human-robot collaboration in industrial environments. *IEEE Access* **5**, 26754–26773 (2017).
2. M. Vasic, A. Billard, Safety issues in human-robot interactions, in *2013 IEEE International Conference on Robotics and Automation (ICRA)* (IEEE, 2013), pp. 197–204.
3. P. Polygerinos, N. Correll, S. A. Morin, B. Mosadegh, C. D. Onal, K. Petersen, M. Cianchetti, M. T. Tolley, R. F. Shepherd, Soft robotics: Review of fluid-driven intrinsically soft devices; manufacturing, sensing, control, and applications in human-robot interaction. *Adv. Eng. Mater.* **19**, 1700016 (2017).
4. O. Yasa, Y. Toshimitsu, M. Y. Michelis, L. S. Jones, M. Filippi, T. Buchner, R. K. Katzschmann, An overview of soft robotics. *Annu. Rev. Cont. Robot. Auton. Syst.* **6**, 1–29 (2023).
5. C. Lee, M. Kim, Y. J. Kim, N. Hong, S. Ryu, H. J. Kim, S. Kim, Soft robot review. *Int. J. Cont. Autom. Syst.* **15**, 3–15 (2017).
6. G. M. Whitesides, Soft robotics. *Angew. Chem. Int. Ed.* **57**, 4258–4273 (2018).
7. M. S. Xavier, C. D. Tawk, A. Zolfagharian, J. Pinskier, D. Howard, T. Young, J. Lai, S. M. Harrison, Y. K. Yong, M. Bodaghi, A. J. Fleming, Soft pneumatic actuators: A review of design, fabrication, modeling, sensing, control and applications. *IEEE Access* **10**, 59442–59485 (2022).
8. F. Ilievski, A. D. Mazzeo, R. F. Shepherd, X. Chen, G. M. Whitesides, Soft robotics for chemists. *Angew. Chem.* **123**, 1930–1935 (2011).
9. S. Zaidi, M. Maselli, C. Laschi, M. Cianchetti, Actuation technologies for soft robot grippers and manipulators: A review. *Curr. Robot. Rep.* **2**, 355–369 (2021).
10. Z. Samadikhoshkho, K. Zareinia, F. Janabi-Sharifi, A brief review on robotic grippers classifications, in *2019 IEEE Canadian Conference of Electrical and Computer Engineering (CCECE)* (IEEE, 2019), pp. 1–4.
11. Z. Wang, K. Or, S. Hirai, A dual-mode soft gripper for food packaging. *Robot. Autonom. Syst.* **125**, 103427 (2020).
12. H. K. Yap, H. Y. Ng, C.-H. Yeow, High-force soft printable pneumatics for soft robotic applications. *Soft Robot.* **3**, 144–158 (2016).
13. D. Yang, M. S. Verma, J.-H. So, B. Mosadegh, C. Keplinger, B. Lee, F. Khashai, E. Lossner, Z. Suo, G. M. Whitesides, Buckling pneumatic linear actuators inspired by muscle. *Adv. Mater. Technol.* **1**, 1600055 (2016).
14. T. J. Wallin, J. Pikul, R. F. Shepherd, 3D printing of soft robotic systems. *Nat. Rev. Mater.* **3**, 84–100 (2018).
15. A. Zatopa, S. Walker, Y. Menguc, Fully soft 3D-printed electroactive fluidic valve for soft hydraulic robots. *Soft Robot.* **5**, 258–271 (2018).
16. N. Bira, Y. Mengüç, J. R. Davidson, 3D-printed electroactive hydraulic valves for use in soft robotic applications, in *2020 IEEE International Conference on Robotics and Automation (ICRA)* (IEEE, 2020), pp. 11200–11206.
17. S. Xu, Y. Chen, N. P. Hyun, K. P. Becker, R. J. Wood, A dynamic electrically driven soft valve for control of soft hydraulic actuators. *Proc. Natl. Acad. Sci. U.S.A.* **118**, e2103198118 (2021).
18. Y. Zhai, A. de Boer, J. Yan, B. Shih, M. Faber, J. Speros, R. Gupta, M. T. Tolley, Desktop fabrication of monolithic soft robotic devices with embedded fluidic control circuits. *Sci. Robot.* **8**, eadg3792 (2023).
19. S. Song, S. Joshi, J. Paik, CMOS-inspired complementary fluidic circuits for soft robots. *Adv. Sci. (Weinh.)* **8**, e2100924 (2021).
20. S. Hoang, K. Karydis, P. Brisk, W. H. Grover, A pneumatic random-access memory for controlling soft robots. *PLOS ONE* **16**, e0254524 (2021).
21. S. T. Mahon, A. Buchoux, M. E. Sayed, L. Teng, A. A. Stokes, Soft robots for extreme environments: Removing electronic control, in *RoboSoft 2019, 2019 IEEE International Conference on Soft Robotics* (IEEE, 2019), pp. 782–787.
22. Q. Jiang, Z. Hu, Y. Xie, K. Wu, S. Zhang, Z. Wu, Liquid-metal-based magnetic controllable soft microswitch with rapid and reliable response for intelligent soft systems. *Micromachines (Basel)* **13**, 2255 (2022).
23. P. Rothemund, A. Ainla, L. Belding, D. J. Preston, S. Kurihara, Z. Suo, G. M. Whitesides, A soft, bistable valve for autonomous control of soft actuators. *Sci. Robot.* **3**, eaar7986 (2018).
24. K. Luo, P. Rothemund, G. M. Whitesides, Z. Suo, Soft kink valves. *J. Mech. Phys. Solids* **131**, 230–239 (2019).
25. D. J. Preston, P. Rothemund, H. J. Jiang, M. P. Nemitz, J. Rawson, Z. Suo, G. M. Whitesides, Digital logic for soft devices. *Proc. Natl. Acad. Sci. U.S.A.* **116**, 7750–7759 (2019).
26. M. P. Nemitz, C. K. Abrahamsson, L. Wille, A. A. Stokes, D. J. Preston, G. M. Whitesides, Soft non-volatile memory for non-electronic information storage in soft robots, in *2020 3rd IEEE International Conference on Soft Robotics (RoboSoft)* (IEEE, 2020), pp. 7–12.
27. D. J. Preston, H. J. Jiang, V. Sanchez, P. Rothemund, J. Rawson, M. P. Nemitz, W.-K. Lee, Z. Suo, C. J. Walsh, G. M. Whitesides, A soft ring oscillator. *Sci. Robot.* **4**, (2019).
28. D. Drotman, S. Jadhav, D. Sharp, C. Chan, M. T. Tolley, Electronics-free pneumatic circuits for controlling soft-legged robots. *Sci. Robot.* **6**, eaay2627 (2021).
29. S. V. Kendre, L. Whiteside, T. Y. Fan, J. A. Tracz, G. T. Teran, T. C. Underwood, M. E. Sayed, H. J. Jiang, A. A. Stokes, D. J. Preston, G. M. Whitesides, M. P. Nemitz, The soft compiler: A web-based tool for the design of modular pneumatic circuits for soft robots. *IEEE Robot. Autom. Lett.* **7**, 6060–6066 (2022).
30. J. D. Hubbard, R. Acevedo, K. M. Edwards, A. T. Alsharhan, Z. Wen, J. Landry, K. Wang, S. Schaffer, R. D. Sochol, Fully 3D-printed soft robots with integrated fluidic circuitry. *Sci. Adv.* **7**, eabe5257 (2021).
31. F. Esser, F. Krüger, T. Masselter, T. Speck, Characterization of biomimetic peristaltic pumping system based on flexible silicone soft robotic actuators as an alternative for technical pumps, in *Biomimetic and Biohybrid Systems. Living Machines 2019*, U. Martinez-Hernandez, V. Vouloutsi, A. Mura, M. Mangan, M. Asada, T. J. Prescott, P. F. M. J. Verschure, Eds. (Springer International Publishing AG, 2019), pp. 101–113.
32. E. H. Skorina, M. Luo, W. Y. Oo, W. Tao, F. Chen, S. Youssefian, N. Rahbar, C. D. Onal, Reverse pneumatic artificial muscles (rPAMs): Modeling, integration, and control. *PLOS ONE* **13**, e0204637 (2018).
33. H. Zhao, Y. Li, A. Elsamadisi, R. Shepherd, Scalable manufacturing of high force wearable soft actuators. *Extreme Mech. Lett.* **3**, 89–104 (2015).
34. G. Miron, B. Bédard, J.-S. Plante, Sleeved bending actuators for soft grippers: A durable solution for high force-to-weight applications. *Actuators* **7**, 40 (2018).
35. R. Hisatomi, T. Kanno, T. Miyazaki, T. Kawase, K. Kawashima, Development of forceps manipulator using pneumatic soft actuator for a bending joint of forceps tip, in *2019 IEEE/SICE International Symposium on System Integration (SII)* (IEEE, 2019), pp. 695–700.
36. D. Drotman, S. Jadhav, M. Karimi, P. de Zonia, M. T. Tolley, 3D printed soft actuators for a legged robot capable of navigating unstructured terrain, in *IEEE International Conference on Robotics and Automation (ICRA)* (IEEE, 2017), pp. 5532–5538.
37. D. Drotman, M. Ishida, S. Jadhav, M. T. Tolley, Application-driven design of soft, 3-D printed, pneumatic actuators with bellows. *IEEE/ASME Trans. Mechatron.* **24**, 78–87 (2019).
38. S. Conrad, T. Speck, F. Tauber, Multi-material 3D-printer for rapid prototyping of bio-inspired soft robotic elements, in *Biomimetic and Biohybrid Systems. Living Machines 2020*, V. Vouloutsi, A. Mura, M. Mangan, F. Tauber, T. Speck, T. J. Prescott, P. F. M. J. Verschure, Eds. (Springer International Publishing AG, 2020), pp. 46–54.
39. S. Conrad, T. Speck, F. J. Tauber, Multi-material FDM 3D printed arm with integrated pneumatic actuator, in *Biomimetic and Biohybrid Systems. Living Machines 2022*, A. Hunt, V. Vouloutsi, K. Moses, R. Quinn, A. Mura, T. J. Prescott, P. F. M. J. Verschure, Eds. (Springer International Publishing, ed. 1, 2022), pp. 27–31.
40. S. Conrad, T. Speck, F. J. Tauber, Tool changing 3D printer for rapid prototyping of advanced soft robotic elements. *Bioinspir. Biomim.* **16**, 055010 (2021).
41. Recreus Industrial S.L., Technical Data Sheet Filaflex 60A 'Pro'; https://drive.google.com/drive/folders/1pn87sLUkfVwzr6DXZcoTYlePyjuE6S0x.
42. Recreus Industrial S.L., Technical Data Sheet Filaflex 70A Ultra-Soft; https://drive.google.com/drive/folders/1b1YqUSY3u4PbGNSWM9uAjZ0HrjZGHYKv.
43. Recreus Industrial S.L., Technical Data Sheet Filaflex 82A Original; https://drive.google.com/drive/folders/1_AFXbDuUfFfOOaafvPbDihpd7lZbgRng.

Acknowledgments: We thank our colleagues from Cluster of Excellence "Living, Adaptive and Energy-autonomous Materials Systems (*liv*MatS @ FIT)" for the interdisciplinary exchange and the many fruitful discussions. We thank the reviewers for their constructive criticism for the improvement of our manuscript. Our thanks also goes to L. Mahoney of *liv*MatS Writer's Studio for improving the English of our manuscript. **Funding:** This work was funded by the Deutsche Forschungsgemeinschaft (DFG, German Research Foundation) under Germany's Excellence Strategy—EXC-2193/1—390951807. **Author contributions:** Conceptualization: S.C., F.J.T., and T.S. Methodology: S.C. and J.T. Investigation: S.C., J.T., P.A., N.K., K.U., and D.B. Visualization: S.C., J.T., and K.U. Funding acquisition: T.S. Project administration: T.S. and F.J.T. Supervision: T.S. and F.J.T. Writing—original draft: S.C. Writing—review and editing: S.C., J.T., P.A., N.K., D.B., F.J.T., and T.S. All authors contributed to and agree with the content of the final version of the manuscript. **Competing interests:** The authors declare that they have no competing interests. **Data and materials availability:** All data are available in the main text or the Supplementary Materials. The data are available via the data repository Dryad at https://doi.org/10.5061/dryad.jq2bvq8gv.

Submitted 7 March 2023
Accepted 2 January 2024
Published 31 January 2024
10.1126/scirobotics.adh4060

Science Robotics

3D-printed digital pneumatic logic for the control of soft robotic actuators

S. Conrad, J. Teichmann, P. Auth, N. Knorr, K. Ulrich, D. Bellin, T. Speck, and F. J. Tauber

Sci. Robot. **9** (86), eadh4060. DOI: 10.1126/scirobotics.adh4060

Science Robotics (ISSN 2470-9476) is published by the American Association for the Advancement of Science. 1200 New York Avenue NW, Washington, DC 20005. The title *Science Robotics* is a registered trademark of AAAS.